

# Experimental tests of pseudo-complex General Relativity

T. Schöenbach<sup>1</sup>, G. Caspar<sup>1</sup>, Peter O. Hess<sup>1,2</sup>,  
Thomas Boller<sup>3</sup>, Andreas Müller<sup>4</sup>, Mirko Schäfer<sup>1</sup> and Walter Greiner<sup>1</sup>

<sup>1</sup>*Frankfurt Institute for Advanced Studies, Johann Wolfgang Goethe Universität,  
Ruth-Moufang-Str. 1, 60438 Frankfurt am Main, Germany*

<sup>2</sup>*Instituto de Ciencias Nucleares, UNAM, Circuito Exterior, C.U.,  
A.P. 70-543, 04510 México D.F., Mexico*

<sup>3</sup>*Max-Planck Institute for Extraterrestrial Physics,  
Giessenbachstrasse, 85748 Garching*

<sup>4</sup>*Excellence Cluster Universe, TU München,  
Boltzmannstrasse 2, 85748 Garching*

March 9, 2022

## Abstract

Based on previous publications exploring pseudo-complex General Relativity (pc-GR) we present a selection of observable consequences of pc-GR and possible ways to experimentally access them. Whenever possible we compare the results to Einstein's GR and differences are worked out in detail. We propose experimental tests to check the predictions of pc-GR for the orbital frequency of test particles, the gravitational redshift effect and the last stable orbit. We will show that the orbital frequency of test particles at a given radius in pc-GR is in general lower compared to standard GR. Also the effect of frame dragging is modified (weakened) in pc-GR. Concerning the gravitational redshift of a radiation emitting object we find that it is also lower in pc-GR than in standard GR. Eventually the classical concept of a last stable orbit has to be modified in pc-GR.

## 1 Introduction

The theory of General Relativity (GR) has up to now withstood all experimental tests. Nevertheless, there are extreme situations in GR, like the formation of a singularity at the center of a black hole, where one expects that quantum effects set in. The existence of a black hole itself is another example for such an extreme situation as there is a part of space which is excluded from the access of an external, even nearby, observer. The event horizon, which for a non-rotating object is predicted in the external Schwarzschild solution of GR at the Schwarzschild radius  $r_S$ , divides space into two parts, one for  $r < r_S$  and the other one for  $r > r_S$ . Though, an infalling observer can access the internal region  $r < r_S$ , this part of space is inaccessible for an outside observer at a *fixed* distance. Such an observer cannot extract information from the inside region while staying outside. This is one reason to search for possible extensions to GR which avoid the appearance of an event horizon, making the internal region accessible for an external observer at a *fixed* distance. Such a theory was proposed by [1] and modified by [2]. An algebraic extension of GR to pseudo-complex (pc) variables was proposed, called pseudo-complex General Relativity (pc-GR). (In [3] it was shown that the only possible extension of GR to different coordinates, avoiding so called ‘ghost solutions’, is the pseudo-complex extension.) One of the important consequences of pc-GR theory is the presence of an energy-momentum tensor in the Einstein equation, which corresponds to the distribution of a field with repulsive properties. It is something similar to dark energy. This energy accumulates at mass distributions and increases when the mass density gets larger. One has to distinguish this effect from the one that a cosmological constant  $\Lambda$  has. The term in the metric containing the cosmological constant is proportional to  $r^2$  and thus increases for greater distances. Therefore it is relevant on cosmological scales. In contrast, the gravitational repulsion in pc-GR can also get stronger for smaller distances. This then has the effect that for very large masses the gravitational collapse is stopped and something what we call a ‘gray star’ is formed instead of a black hole. The pc-GR theory does not predict an event horizon, and thus the space with  $r < r_S$  is accessible for an external observer. In [2] the pc-GR solutions for a non-

rotating gray star (Schwarzschild), a charged gray star (Reissner-Nordström) and a rotating gray star (Kerr) were discussed. In [4] the theory was applied to the Robertson-Walker model of the universe, encountering new solutions, for example, a finite or vanishing acceleration of the Universe for very large times.

It is important to investigate further cases, which can be verified by experiments, for example by observing quasiperiodic oscillations due to orbital motions around a central large mass, see [5, 6, 7]. Very recently, a dense gas cloud has been detected falling into the aggregation zone of the Galactic Center, see [8]. The gas will be aggregated by the Galactic Center from 2013 onwards, and as the lower limit of the absolute value of the black hole spin  $|a|$  is larger than  $0.5m$  this will allow for additional tests of theories in the strong field limit.

Our pc-GR theory and standard GR make different predictions concerning the angular velocity of test particles close to a large central mass. Experimental tests of those predictions are discussed in this contribution. The hope is that in the near future, it will be possible to detect phenomena in regions near the event horizon of standard GR. The predictions of our pc-General Relativity, which deviate from the standard General Relativity theory then can be compared to experimental results.

This paper is organized as follows: In section 2 we give a very short summary on pseudo-complex variables and pc-GR. In section 3 some experimental tests are proposed. We examine 1) the orbital frequency of a particle around a gray star, 2) the radial dependence of the redshift, 3) the structure of the effective potential for the Schwarzschild and Kerr solutions, and finally a discussion of the last stable orbit around a gray star. In all cases, we compare our results to the the predictions of standard GR. Finally, in section 4 we present our conclusions.

In this article we use the signature  $(+,-,-,-)$  for the metric, together with the definition of the Riemann tensor which leads to the Einstein equations in the form  $G_{\mu\nu} = \mathcal{R}_{\mu\nu} - \frac{1}{2}g_{\mu\nu}\mathcal{R} = -\frac{8\pi\kappa}{c^4}T_{\mu\nu}$ , with  $c$  being the speed of light and  $\kappa$  the gravitational constant. The parameter  $a$  containing the angular momentum  $J$  of a rotating compact massive object, is defined as  $a = \frac{-\kappa J}{mc^3}$  like in [9]. Here  $m$  is half the Schwarzschild radius of the considered object. It is related to the mass  $M$  of the object by  $\frac{\kappa M}{c^2} = m \equiv \frac{r_s}{2}$ . The parameter  $a$  has units of length and will be measured in multiples of  $m$ .

## 2 Pseudo-complex General Relativity

In what follows, a short review of the main properties of pc-GR is given. The pseudo-complex coordinates are  $X^\mu = x^\mu + I \frac{l}{c} u^\mu$ , with  $x^\mu$  as the position and  $u^\mu$  as a vector with units of a four-velocity. The factor  $l$  is introduced due to dimensional reasons. It represents a minimal length parameter.  $c$  is the speed of light. An important property is that a pseudo-holomorphic function of pc-variables can be written as  $F(X) = F_+(X_+) \sigma_+ + F_-(X_-) \sigma_-$  ( $X_\pm^\mu = x^\mu \pm \frac{l}{c} u^\mu$ ), with  $\sigma_\pm = \frac{1}{2} (1 \pm I)$ ,  $\sigma_\pm^2 = \sigma_\pm$  and  $\sigma_+ \sigma_- = 0$ . Due to the last relation, pc-variables have a zero-divisor<sup>1</sup> with  $\sigma_\pm$  as its basis. Calculations can be done independently in the  $\sigma_+$  or  $\sigma_-$  component. This plays a crucial role for the pc-extension of GR. For more details on pc-variables and rules of calculations, see [10, 11].

In pc-GR the metric is pseudo-complex and written as  $g_{\mu\nu}(X) = g_{\mu\nu}^+(X_+) \sigma_+ + g_{\mu\nu}^-(X_-) \sigma_-$ . Due to the fact that calculations can be performed independently in each  $\sigma_\pm$  component, a GR theory is constructed in each component. All rules can be immediately copied from any text book on GR, e.g. [12, 9]. An important ingredient is the modification of the variational principle, first proposed in [13, 14]. The variation of the action is now equal to a value within the zero divisor, i.e.  $\delta S$  is either proportional to  $\sigma_+$  or  $\sigma_-$ , where for convenience the  $\sigma_-$  is chosen (to take  $\sigma_+$  just gives an equivalent description where plus and minus are interchanged). This modifies the Einstein equations which are now

$$G_{\mu\nu} = -\frac{8\pi\kappa}{c^2} T_{\mu\nu} \sigma_- \quad . \quad (1)$$

This represents a trivial extension to standard GR, keeping the beautiful structure of the theory, only adding an energy-momentum tensor, similar to theories which include matter. The energy-momentum tensor describes the contribution of a field which has repulsive properties and is responsible for the halt of a gravitational collapse. Finally, the metric  $g_{\mu\nu}(X)$ , obtained in an actual case, is projected to  $g_{\mu\nu}(x)$ , where the function is the same but the pc-variables are substituted by the coordinates and the pc-parameters by their pseudo-real components. This corresponds to neglecting the contributions due to the minimal length  $l$ , see [2]. We will not repeat the details here, but rather refer the reader to the references [1, 2].

---

<sup>1</sup>For a commutative ring the zero-divisor is the set of numbers  $a, b$  which fulfill the relation  $a \cdot b = 0$  without being zero on their own.

The form of the energy-momentum tensor might be explained by microscopic physics [15, 16, 17], where the vacuum fluctuations (Casimir effect) are discussed in the presence of matter. The Schwarzschild metric is treated as a background and the influence of the matter on the vacuum fluctuation is deduced, using different approaches for the vacuum. A strongly decreasing energy density as a function of distance is found. The same should be repeated taking into account the coupling of the vacuum fluctuations with the metric. We mention this work here, because it shows that our ansatz has a possible microscopic origin.

The following solution of equation (1) is the pseudo-complex analogue of the Kerr metric of standard GR

$$\begin{aligned}
g_{00}^{\text{K}} &= \frac{r^2 - 2mr + a^2 \cos^2 \vartheta + \frac{B}{2r}}{r^2 + a^2 \cos^2 \vartheta} \\
g_{11}^{\text{K}} &= -\frac{r^2 + a^2 \cos^2 \vartheta}{r^2 - 2mr + a^2 + \frac{B}{2r}} \\
g_{22}^{\text{K}} &= -r^2 - a^2 \cos^2 \vartheta \\
g_{33}^{\text{K}} &= -(r^2 + a^2) \sin^2 \vartheta - \frac{a^2 \sin^4 \vartheta (2mr - \frac{B}{2r})}{r^2 + a^2 \cos^2 \vartheta} \\
g_{03}^{\text{K}} &= \frac{-a \sin^2 \vartheta 2mr + a \frac{B}{2r} \sin^2 \vartheta}{r^2 + a^2 \cos^2 \vartheta} \quad , \tag{2}
\end{aligned}$$

which reduces in the limit  $a = 0$  to the pseudo-complex analogue of the standard GR Schwarzschild solution

$$\begin{aligned}
g_{00}^{\text{S}} &= \left(1 - \frac{2m}{r} + \frac{B}{2r^3}\right) \\
g_{11}^{\text{S}} &= -\left(1 - \frac{2m}{r} + \frac{B}{2r^3}\right)^{-1} \\
g_{22}^{\text{S}} &= -r^2 \\
g_{33}^{\text{S}} &= -r^2 \sin^2 \vartheta \quad . \tag{3}
\end{aligned}$$

Here the superscripts ‘S’ and ‘K’ refer to ‘Schwarzschild’ and ‘Kerr’, respectively. In the further discussions we omit these superscripts, as a distinction between Schwarzschild and Kerr metric can be made via the parameter  $a$ , which is a measure of the rotation of the object, see [9, 12].

Requiring a positive  $g_{00}$ -component of the metric leads to a lower possible limit  $B > B_{\min} = \frac{64}{27}m^3$ . In deriving the metric, we have to make special

assumptions about the energy-momentum tensor. As discussed in [2], a fluid model for the dark energy is used. The density is assumed to be proportional to  $1/r^5$ , in order that the additional metric component behaves as  $1/r^3$ . The reason for this lies in astronomical observations in the solar system [18] where contributions of the order  $1/r^2$  are already excluded. In general, for the additional metric contribution one can use a power expansion in  $1/r$ , starting with  $1/r^3$ . This includes more parameters and for that reason, keeping the extended theory as simple as possible, we take for the moment only the leading term. Thus, only one additional parameter is included, as expected when a theory is generalized. The effects of changing the parameter  $B$  and the power in  $1/r$  are discussed in the corresponding places of this article.

The pc-GR theory also eliminates the singularity at  $r = 0$ . There, the metric component  $g_{00}$  diverges in ordinary GR. Therefore, the theory presents a different suggestion on how to avoid the singularity at the center. However, this is only of academic interest, because the massive object ceases contraction below the position of the minimum of the effective potential, which is proportional to  $g_{00}$ . For radial distances smaller than the position of the minimum of  $g_{00}$  mass should be present, which has to be taken into account, changing the metric. This is the subject of our current investigation, important also for neutron stars. For  $r$  near the origin, quantum effects will have to be taken into account, but this is not considered in the current work. The singularity problem is *not the topic discussed in this contribution* but rather we investigate the consequences of the disappearance of the event horizon as for example done by [19].

## 3 Experimental tests

### 3.1 Radial dependence of the angular frequency $\omega(r)$

The observation of the circular movement of matter around a large central mass might give hints for deviations of pc-GR from Einstein's GR. For example, the orbital frequency of a plasma cloud can be measured. We expect a spectacular infall event of such a plasma cloud very soon [8] allowing to test GR very close to a black hole candidate. Indeed, this is already possible, because flares are observed at the Galactic center black hole candidate Sgr A\*, see [5, 6].

We approximate such clouds by a massless particle and therefore calculate

first the angular frequency  $\omega(r)$  of a point particle orbiting a large central mass  $M$  on a stable geodesic track, see [2]. The following discussion is related to subsection 3.3, where the existence of a last stable orbit is investigated. In order to determine the angular velocity, we proceed similar to [2] and follow the book of Adler et al. [9], using the Lagrange function

$$L = g_{00}c^2\dot{t}^2 + g_{11}\dot{r}^2 + g_{22}\dot{\vartheta}^2 + g_{33}\dot{\varphi}^2 + 2g_{03}c\dot{t}\dot{\varphi} = \frac{ds^2}{ds^2} = 1 \quad , \quad (4)$$

where the dot represents  $\frac{d}{ds}$  and  $s$  is a curve parameter, e.g. the eigentime. The variation of  $L$  then yields the geodesic equations from which we will use the radial one:

$$\frac{d}{ds}(2g_{11}\dot{r}) = g'_{00}c^2\dot{t}^2 + g'_{11}\dot{r}^2 + g'_{22}\dot{\vartheta}^2 + g'_{33}\dot{\varphi}^2 + 2g'_{03}c\dot{t}\dot{\varphi} \quad . \quad (5)$$

Here the prime ' stands for the derivative  $\frac{\partial}{\partial r}$ . To simplify the calculations we restrict our discussion to motions in the equatorial plane at a constant distance to the central object, e.g.  $r = r_0$ ,  $\dot{r} = 0$ ,  $\vartheta = \frac{\pi}{2}$  and  $\dot{\vartheta} = 0$ . In this case, equation (5) becomes

$$0 = g'_{00}(r_0)c^2\dot{t}^2 + g'_{33}(r_0)\omega^2\dot{t}^2 + 2g'_{03}(r_0)\omega c\dot{t}^2 \quad , \quad (6)$$

where we introduced the angular frequency  $\omega = \frac{d\varphi}{dt} = \frac{\dot{\varphi}}{\dot{t}}$ .

Obviously equation (6) is a quadratic equation in  $\omega$  with the two solutions

$$\omega_{\pm} = c \frac{-g'_{03} \pm \sqrt{(g'_{03})^2 - g'_{00}g'_{33}}}{g'_{33}} \quad . \quad (7)$$

Inserting now equation (2) yields

$$\omega_{\pm} = c \frac{-ah(r) \pm \sqrt{2rh(r)}}{-2r + -a^2h(r)} = \frac{c\sqrt{h(r)}}{-a\sqrt{h(r)} \mp \sqrt{2r}} \quad , \quad (8)$$

with

$$h(r) = \frac{2m}{r^2} - \frac{3B}{2r^4} \quad . \quad (9)$$

For  $h(r) > 0$ , equation (8) has two real solutions, one for co- and one for counter-rotation with respect to the rotating central body. Note that  $h(r) >$

0 is equivalent to  $r^2 > (3B)/(4m)$ , which gives  $r > (4/3)m$  for  $B = B_{\min}$ . The task now is to find out which solution of equation (8) corresponds to which physical motion.

The angular momentum of the central mass is given by  $J$ , which might have positive or negative sign. As usual we assign a positive  $J$  to a counter-clockwise rotation (i.e., mathematical positive sense). For convenience we define that the angular momentum for this rotation points towards the North pole of the central mass. Next we have to use the connection between the parameter  $a$  and the angular momentum  $J$  as given in [2, 9] by

$$a = \frac{-\kappa J}{mc^3} \quad . \quad (10)$$

Here one has to be careful as there also exists the convention  $a = +\frac{\kappa J}{mc^3}$  as used for example in [12, 20].

We choose  $J$  to be positive and accordingly  $a$  to be negative. Since  $h(r) > 0$ , it always holds that  $|\omega_+| > |\omega_-|$ . First consider  $2r > a^2 h(r)$ , which is always the case for large  $r$ . In this case  $\omega_+$  is negative and  $\omega_-$  is positive. Consequently  $\omega_-$  describes co-rotating orbits, whereas  $\omega_+$  describes counter-rotating orbits. Now consider  $2r < a^2 h(r)$ , which occurs for small  $r$ . In this case  $\omega_+$  and  $\omega_-$  are both positive, so *the previous counter-rotating orbit has turned into a co-rotating orbit*.

In Fig. 1 the angular frequency  $\omega_-$  of a mass in a co-rotation (prograde) orbit is plotted versus the radial distance, with the rotational parameter  $a = -0.995m$ . In Fig. 2 the same is shown for counter-rotation (retrograde orbit). In this case a last stable orbit exists and the curve ends at a certain minimal value. The radial distance is measured in units of  $m$ , and  $\omega$  in units of  $c/m$ . For a mass of four million times the mass of the sun [5], corresponding to the object at the center of our galaxy, a value of 0.219, at the maximum of  $\omega = 2\pi\nu$  corresponds to a orbital period of 9.4 minutes. In Fig. 1 we observe a maximum orbital frequency below  $r = 2$ , i.e. below the Schwarzschild radius. Rewriting equation (8) as

$$\omega_{\pm} = \frac{c}{-a \mp \sqrt{\frac{2r}{h(r)}}} \quad , \quad (11)$$

we recognize that the position of this maximum frequency is *independent of the value of  $a$* . This is an important finding, because once a maximum in  $\omega_-$  is observed, the position of this maximum together with the mass will determine



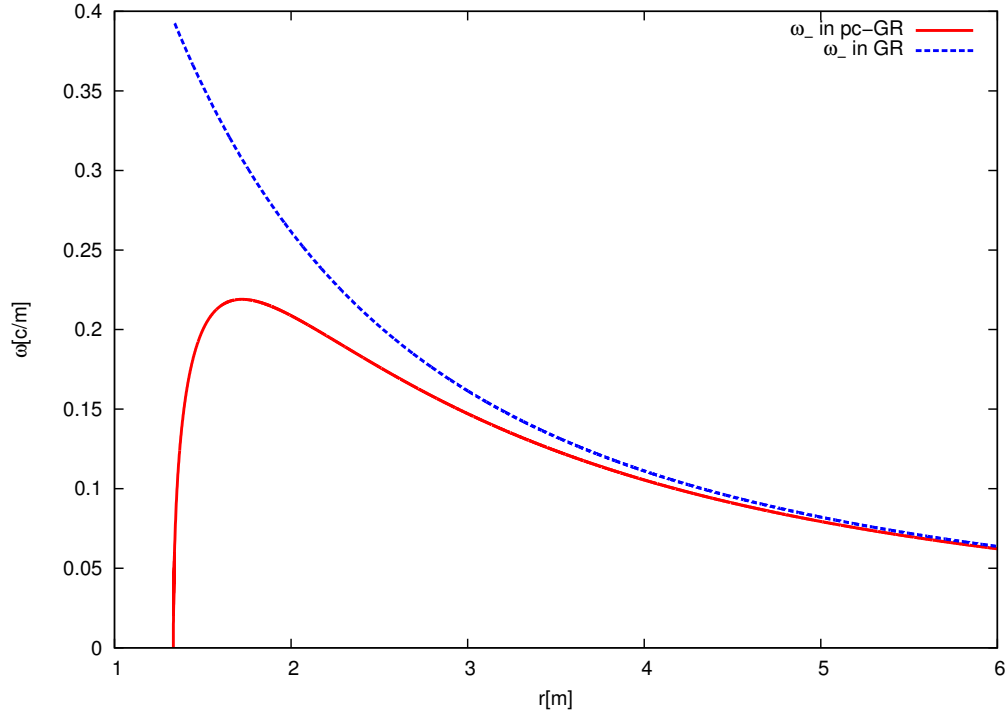


Figure 1: Orbital frequency as a function of  $r$ , for stable geodesic prograde (rotating in the same way as the central massive object) circular motion. The value  $\omega = 0.219$ , for a gray star having mass  $4 \times 10^6$  solar mass, corresponds to about 9.4 minutes for a full circular orbit. This plot is made with parameter values of  $a = -0.995m$  and  $B = \frac{64}{27}m^3$ .

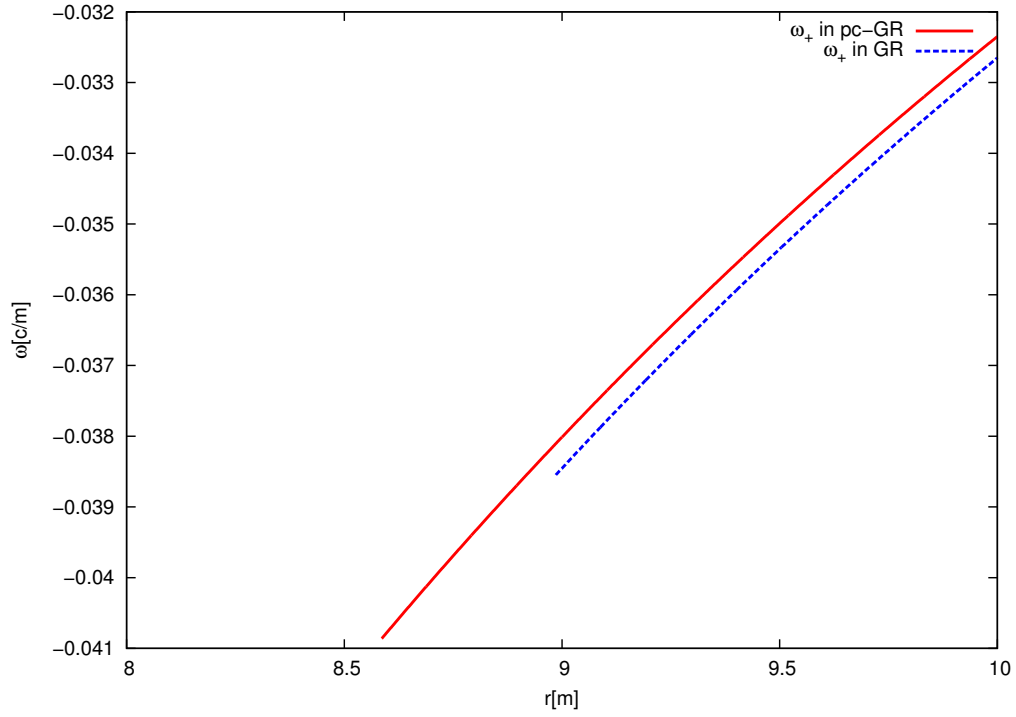


Figure 2: Orbital frequency as a function of  $r$ , for retrograde (rotating in the opposite way as the central massive object) circular motion. The parameters for this plot are  $a = -0.995m$  and  $B = \frac{64}{27}m^3$ .

$B$ . It is given by the minimum of  $r/h(r)$ , which can be easily calculated to occur at  $r = \sqrt{5B/4m}$ . For  $B = B_{\min}$  we obtain  $r = \sqrt{80/27}m \approx 1.72m$ , in perfect agreement with the numerical value in Fig. 1. Starting below about 2 Schwarzschild radii, differences between the standard GR and the pc-GR appear, which become noticeable near  $r = 2m = r_s$ . In general, for a particle it takes more time to circle the center in pc-GR than in GR. This difference is expected to be observable in the near future. Care has to be taken though, because in standard GR the difference from pc-GR can masquerade as a different (false) radius or a different value for  $a$ . Therefore, one has to combine this observation with the measurement of the redshift, which also depends on the radial distance. Only if the same radial distance is obtained in both cases, consistency is achieved. As will be shown in the last subsection, a stable orbit for prograde motion always exists. In the case of retrograde orbits we do not expect to see big differences as a last stable orbit exists at  $r > 8m$  (for  $a = -0.995m$ ). Below that value there are no stable orbits anymore (see section 3.3 for details). But in this region of space the difference between GR and pc-GR is extremely small.

When instead of the  $1/r^3$  dependence in the additional term in the metric a higher power is considered, the qualitative behavior of the curve in Fig. 1 does not change, although the maximum is shifted. One can show that for a correction of order  $1/r^n$  the maximum occurs at  $r_{max} = \sqrt[n]{(n(n+2)B)/12m}$ . For constant  $B$  and  $m$  this leads to increasing  $r_{max}$ , until around  $n = 10$  the value of  $r_{max}$  decreases again and around  $n = 25$  reobtains its value as for  $n = 3$ . Also  $B_{\min}$  does depend on  $n$  as  $B_{\min}/2 = (2m/n)^n(n-1)^{n-1}$ .

Up to now we have only considered stable geodesic orbits. But there is also a possibility to derive constraints to the orbital frequencies for more general orbits. Following Misner et al. [12] we consider the demand that the line element

$$ds^2 = g_{00}c^2 dt^2 + g_{11}dr^2 + g_{22}d\vartheta^2 + g_{33}d\varphi^2 + 2g_{03}cdtd\varphi \quad (12)$$

is positive (The difference is that up to now the Lagrangian (4) was varied in order to obtain the geodesic equation, while we consider now the general (non-geodesic) case.). Again we restrict the calculations to circular ( $dr = 0$ ) motions which lie in the equatorial plane ( $d\vartheta = 0$ ,  $\vartheta = \pi/2$ ). The limiting case ( $ds^2 = 0$ ) corresponding to a circularly rotating photon is then given by

$$g_{00}c^2 dt^2 + g_{33}\omega^2 dt^2 + 2g_{03}c\omega dt^2 = 0 \quad , \quad (13)$$

where we denoted again  $\omega = \frac{d\varphi}{dt}$ . Equation (13) is a quadratic equation in  $\omega$  with the following solutions

$$\bar{\omega}_{\pm} = c \frac{-g_{03} \pm \sqrt{(g_{03})^2 - g_{00}g_{33}}}{g_{33}} . \quad (14)$$

Remarkably this is formally the same as equation (7) *but the metric coefficients appear instead of their derivatives*. Inserting equation (2) we get

$$\bar{\omega}_{\pm} = c \frac{af(r) \pm \sqrt{D}}{-(r^2 + a^2) - a^2 f(r)} , \quad (15)$$

with

$$f(r) = \frac{2m}{r} - \frac{B}{2r^3} \\ D = r^2 + a^2 - 2mr + \frac{B}{2r} . \quad (16)$$

In [2] we have shown that for  $B \geq B_{\min} = (4/3)^3 m^3$  it holds  $D \geq 0$ . Therefore,  $\bar{\omega}_{\pm}$  has always two real solutions. It also holds  $f(r) \geq 0$  for  $r \geq (3B)/(4m)$ , that is  $r \geq (4/3)m$  for  $B = B_{\min}$ . Similar to the above discussion, when the power of  $1/r$  is increased, the  $f(r)$  decreases, which in turn increases  $\omega_{\pm}$ . This is modified by the  $\sqrt{D}$  term. When  $B$  increases, also the  $f(r)$  decreases and a similar effect is observed, again modified by the  $\sqrt{D}$  term in the denominator. However, in general the structure remains the same.

We again choose  $J$  positive and accordingly  $a < 0$ . In this case we have  $\bar{\omega}_- > 0$  and  $|\bar{\omega}_-| \geq |\bar{\omega}_+|$ . Thus  $\bar{\omega}_-$  describes the angular frequency of a co-rotating photon. Since for large  $r$  it holds  $D \gg f(r)$ , in this range  $\bar{\omega}_+$  is negative and corresponds to counter-rotation. For smaller  $r$  the term proportional to  $1/r$  leads to an increasing  $f(r)$ , and  $\bar{\omega}_+$  might become zero. In classical GR the sphere where  $\bar{\omega}_+ = 0$  is called the ergosphere. Since  $g_{33} < 0$ , it follows from equation (15) that the radius of the ergosphere is given by the condition  $g_{00} = 0$ . In pc-GR  $g_{00} > 0$  and thus  $\bar{\omega}_+$  is always negative. However, if  $B = B_{\min} + \epsilon$  with  $\epsilon \ll 1$ ,  $\bar{\omega}_+$  can become very close to zero at a certain radius.

The results of equation (15) can be visualized quite nicely. In Fig. 3 one can see the allowed range for circular movement (not necessarily on stable

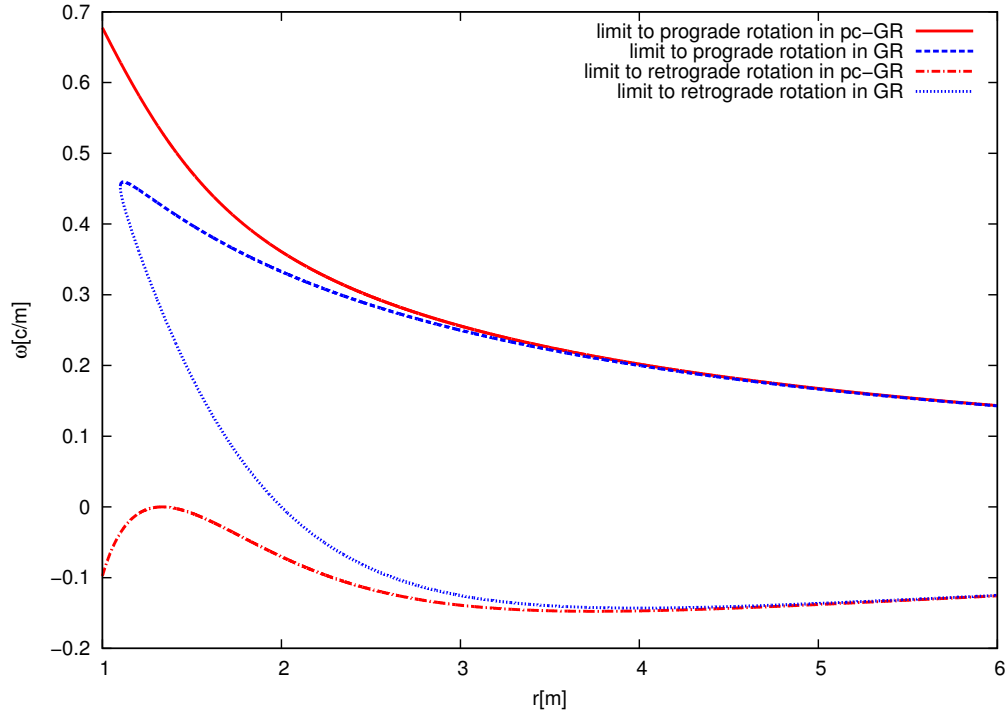


Figure 3: Limits on the orbital frequencies of circular motion in the equatorial plane. The frequencies of particles moving on circular orbits must lie between the limiting curves. The parameters are  $a = -0.995m$  and  $B = \frac{64}{27}m^3$ .

geodesics) compared between pc-GR and Einstein's GR. The curves for pc-GR show a significantly different behavior as those for Einstein's GR. In standard GR there is a certain radius where the ergosphere begins. For smaller radii, particles have to co-rotate with the central mass, see [9, 12]. This behavior can be seen in Fig. 3 as the limiting curve for counter-rotating orbits changes its sign. The curves finally meet at the event horizon, where all particles have to rotate with the same frequency and in the same direction as the black hole (frame-dragging).

This is different in pc-GR. Although the curve for counter-rotating orbits also approaches zero, there is no point where the two limiting curves coincide. In fact the point where the curve for counter-rotating orbits reaches zero also marks a maximum of this curve. It follows that although there is a frame-dragging effect in pc-GR it is very small compared to standard GR in the regime of strong gravitational fields. The allowed range of values for circular motion is greater in pc-GR than in standard GR.

For weak gravitational fields the effect of frame-dragging according to the predictions of [21] has been confirmed experimentally, see [22] and [23]. But these predictions and measurements are not affected by the changes we consider here, as Lense and Thirring use a weak field approximation which stays the same in pc-GR and standard GR, see [2].

Now, we have firm prognoses at hand and we suggest astronomical systems and methods which can be used to test the orbital frequencies. Obvious testbeds are individual objects which orbit the black hole candidate, e.g. something like planets in the solar system. If we would observe a single star orbiting the compact mass we can simply apply GR versions of Kepler's laws. The third law connects central mass, semi-major axis of the elliptical orbit and orbital time, or orbital frequency respectively. If an astronomical observer is lucky enough to glimpse such a close stellar encounter, he could measure both orbital frequency and orbital radius, and put these measurements into the  $\omega$ - $r$  diagram. This would allow a direct test of whether the classical GR black hole or the pc-GR gray star model provides a better fit. Slight modifications may arise when the  $B/r^3$ , as it appears in the metric, is modified to  $B/r^n$ , ( $n > 3$ ), which produces changes as discussed above.

Unfortunately, these stellar encounters are rare events. Typical rates for a massive black hole like the one in the center of our Milky Way are such that one star is swallowed every 10.000 years. Nevertheless, there are known cases where stellar tidal disruption events have been observed, see [24, 25]. Indeed, if a star approaches a critical distance to a black hole [26], then tidal

forces disrupt the star and the stellar material becomes accreted onto the black hole. This leads to an increase in luminosity. Such an event would be observed as an accretion burst accompanied by a luminosity outburst. The so-called S stars are many stars observed in the infrared which orbit the galactic center black hole, see [28]. However, these stars are still too far away from the central mass to serve as probes to discriminate between GR and pc-GR.

Typically, the spatial resolution is not high enough to image details close to the Galactic center black hole. An alternative is to observe flares coming from that region. In fact, flares happen very frequently - typically once per day in the infrared at distances of about 30 Schwarzschild radii, see [5], as well as in X-rays, see [6]. But the nature of the flare emitter is still poorly understood. A common model interprets the flare emission as modulated by relativistic Doppler effects and gravitational redshift, see references [5, 6]. The flare emission oscillates and can be analyzed using power spectra, i.e. Fourier transforms of the emission. Astronomers evaluate the flare frequencies by disentangling the prominent peaks in the power spectrum. Usually, one assumes a rotation of the flare at the last stable orbit. The shape of a spectral line emitted at the last stable orbit is directly related to the black hole spin, see [27]. Therefore, one can deduce the black hole spin by matching the spin-dependent last stable orbit, which is calculated theoretically, with the observed last stable orbit. In fact, this is a common method to measure the spin of a black hole. But the last stable orbit is different if one applies the pc-GR theory, see section 3.3. Hence, the whole analyses done in GR should be repeated in the pc-GR framework to search for a conclusive result. This is in addition motivated by the crucial point that state-of-the-art infrared flare observations of the Galactic center black hole hint for a spin parameter  $a < -0.5m$ , which is not the same as that deduced from the X-ray flares,  $a \sim -0.99m$ . Of course it should be the same black hole (or gray star)! Such measurements will be improved significantly in the future by using the GRAVITY experiment, see [29], in the infrared and new generations of Athena-like X-ray observatories, see [30]. A summary of future near-infrared and X-ray observations to test GR theories in the strong field limit is given by [31].

### 3.2 Gravitational redshift for Schwarzschild- and Kerr-type solutions

The redshift of a spectral feature carries valuable information and can be measured rather easily by astronomers.

Let us consider a light ray, which is sent by a massless particle at rest in free space near a strong gravitational source to an observer at infinity. To calculate the gravitational redshift we need the relation between the proper time and the coordinate time of the observer, which can be extracted from the line element

$$ds^2 = c^2 d\tau^2 = g_{00}c^2 dt^2 + g_{11}dr^2 + g_{22}d\vartheta^2 + g_{33}d\varphi^2 + 2g_{03}cdtd\varphi \quad . \quad (17)$$

Since the particle is considered at rest the equation simplifies to

$$d\tau^2 = g_{00}dt^2 \quad . \quad (18)$$

In most cases we can assume, that the metric does neither change in the time between two wave peaks (here denoted by  $\tau_0$  respectively  $t_{obs}$ ), nor for the space between the particle and the observer while the ray is traveling. In this case the equation can be integrated and the result is obviously

$$\tau_0 = \sqrt{g_{00}}t_{obs} \quad . \quad (19)$$

Furthermore, since the times represent the interval between two wave peaks, they are the inverse of the frequencies in their respective system. Hence the observed frequency differs from the emitted in the following way

$$\nu_{obs} = \sqrt{g_{00}}\nu_0 \quad . \quad (20)$$

Following the convention in the literature, we define the parameter  $z$  to obtain a measure for the redshift

$$z := \frac{\nu_0 - \nu_{obs}}{\nu_{obs}} = \frac{1}{\sqrt{g_{00}}} - 1 \quad . \quad (21)$$

Using equation (3) we get for the pseudo-complex analogue of the Schwarzschild metric

$$z = \frac{1}{\sqrt{1 - \frac{2m}{r} + \frac{B}{2r^3}}} - 1 \quad , \quad (22)$$



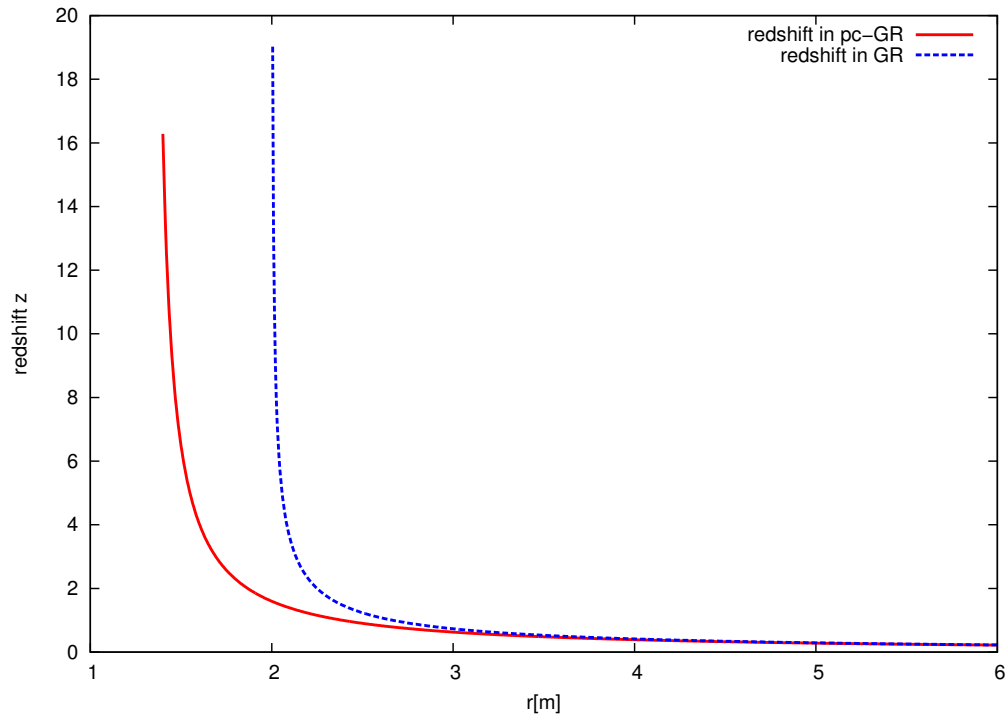


Figure 4: Redshift of an emitter at the position  $r$  in the outside field of a spherically symmetric, uncharged and static mass (Schwarzschild metric) and also for the field at the equator of a rotating mass ( $\vartheta = \frac{\pi}{2}$ ).  $B$  is set to  $\frac{64}{27}m^3$  and  $a = 0.995m$ .

while the redshift in the pc-Kerr metric can be calculated by inserting  $g_{00}$  from equation (2)

$$z = \frac{\sqrt{r^2 + a^2 \cos^2(\vartheta)}}{\sqrt{r^2 - 2mr + a^2 \cos^2(\vartheta) + \frac{B}{2r}}} - 1 \quad . \quad (23)$$

Note that the redshift at the equator ( $\vartheta = \frac{\pi}{2}$ ) of the Kerr solution is exactly equal to that in the Schwarzschild case. This redshift is shown for the limiting case  $B = \frac{64}{27}m^3$  in Fig. 4. One can clearly see, that between two and three gravitational radii pc-GR differs noticeable from standard GR. The pc-GR theory predicts smaller redshifts for the same radius, so we would expect, to be able to look further inside. In this particular case the redshift still diverges at  $r = \frac{4}{3}m$ , but in reality we expect a slightly larger B with the result that the redshift remains finite for the whole space-time. For a larger B, the curve for the redshift in pc-GR remains finite in Fig. 4. In general, the redshift  $z$  is decreased. Also when the power in  $1/r$  is increased, the value of  $z$  decreases. The main structure, however, remains which corresponds to smaller redshifts in pc-GR, compared to GR, especially noticeable near the Schwarzschild radius. In conclusion, we predict that in pc-GR the surface of the central mass could in principle be visible. However it can be strongly obscured due to the gravitational redshift.

Nevertheless this result is not the whole picture for the Kerr solution, since so far we have neglected the dependence on the inclination  $\vartheta$ . Compared to the previous result the other extremes are the poles, i.e.  $\vartheta = 0$  or  $\vartheta = \pi$ . This case is shown in Fig. 5. Here we see a completely different behavior, since the maximal redshift is roughly 1 and the central object should be clearly visible. This means that the observation of a massive object from well separated angles could test our predictions. Figure 6 shows the dependence of the redshift on the inclination  $\vartheta$  for a given radius  $r = 2.05m$ . It thus gives an interpolation between the extremes shown in Fig. 4 and Fig. 5 for a certain radius.

The crucial difference between classical GR black holes and the pc-GR gray stars is that the pc-GR object appears brighter for the same mass. In other words, the prominent feature of a black hole, i.e. its blackness, is reduced in pc-GR. A problem which might arise in this context is that one cannot readily distinguish standard black holes from pc-GR objects because one might mistake a pc-gray star for a standard black hole by underestimating

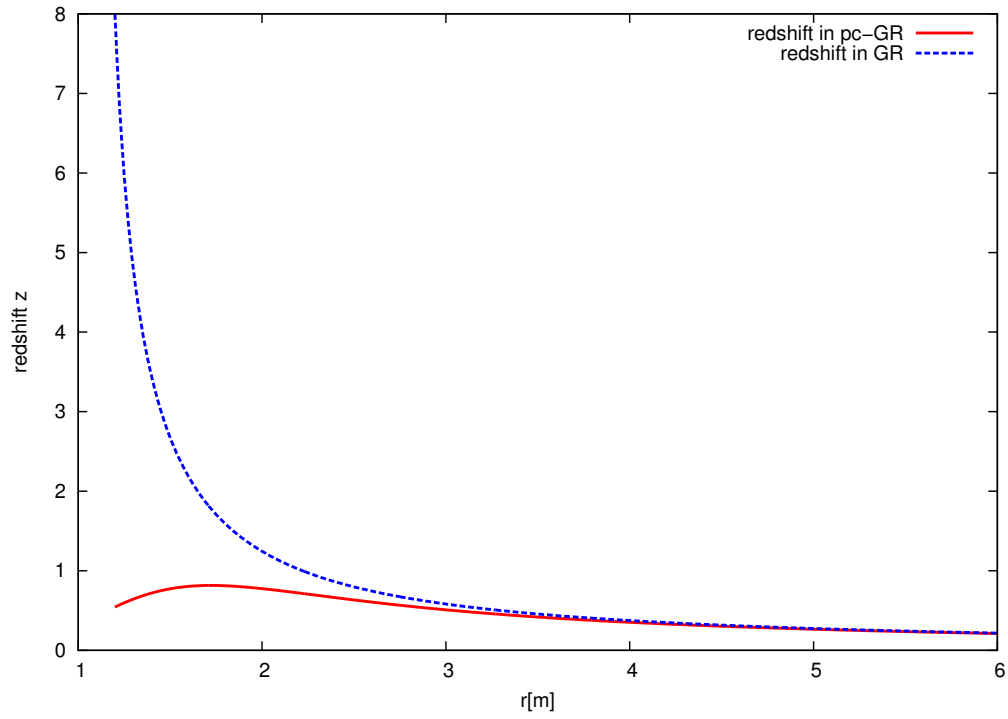


Figure 5: Redshift for an emitter at the position  $r$  in the outside field of an axially symmetric, uncharged and rotating mass (Kerr metric) at the poles (e.g.  $\vartheta = 0$  or  $\vartheta = \pi$ ).  $B$  is again chosen to be  $\frac{64}{27}m^3$  and  $a = 0.995m$ .

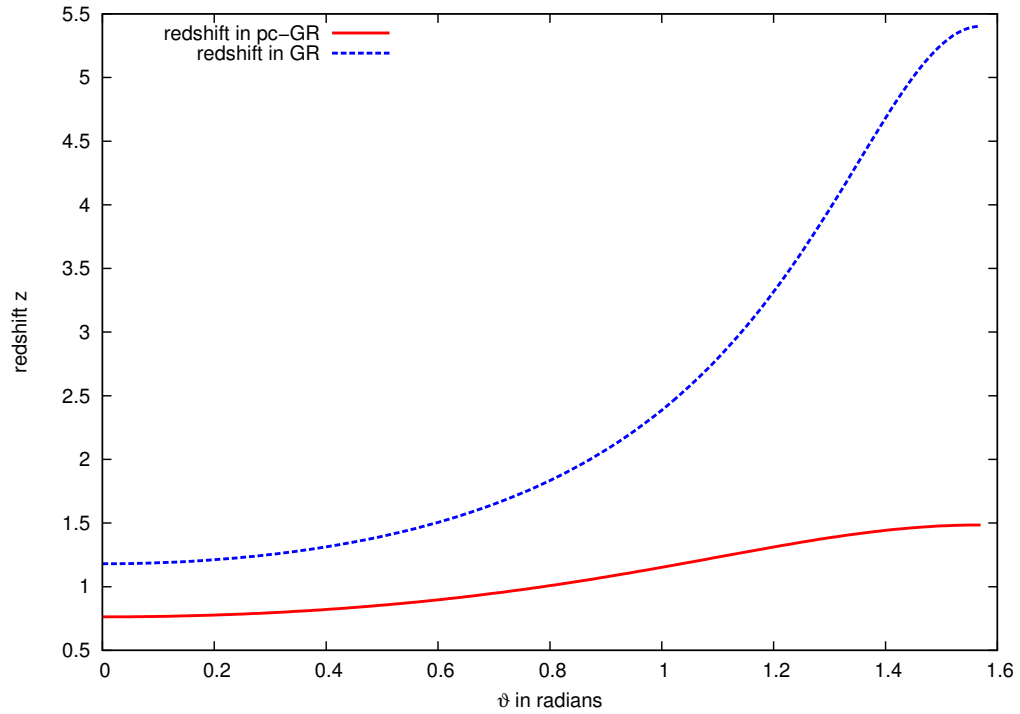


Figure 6: Redshift for an emitter at the radius  $r = 2.05m$  in the outside field of an axially symmetric, uncharged and rotating mass (Kerr metric) for  $\vartheta$  between 0 and  $\frac{\pi}{2}$ .  $B$  is equal to  $\frac{64}{27}m^3$  and  $a = 0.995m$ .

the mass. To prevent this, astronomers should combine various methods to weigh black holes (see e.g. [32] for a review on black hole mass and spin determination).

An obvious method is to image the direct emission from a massive object and its immediate surroundings. For an illustration, see the GR ray tracing simulation in Fig. 7.

The event horizon is proportional to the black hole mass  $M$ , as can be seen from the Schwarzschild radius  $r_S = \frac{2\kappa M}{c^2}$ . Therefore, astronomers could in principle weigh a black hole by measuring the observed black spot. Unfortunately, black holes are very compact objects and the black hole candidates known so far subtend tiny angles on the sky. Only for two nearby massive black-hole candidates are black hole spot measurements currently feasible, i.e. Sgr A\* and M87 in the Virgo cluster. Concerning stellar-mass black hole candidates there seems to be no chance to succeed in applying this techniques - at least with the state-of-the-art generation of detectors. We show this by evaluating the apparent size, i.e. the size of the black hole event horizon as viewed from the distance. The angular scale for imaging the event horizons amounts to micro arc-seconds only. Such a tiny size at the sky can only be imaged by using sophisticated techniques called *Very Long Baseline Interferometry* (VLBI) in radio astronomy. For astrophysics, an interferometer is an array of telescopes observing together astronomical objects. The advantage is that the resolution scales with the distance of the individual telescopes. For VLBI the resolution corresponds to a single telescope which was thousands of kilometers in diameter. Indeed, radio astronomers have the best chance to image a black hole directly. They use these methods also to image the jet launching area in the vicinity of black holes in the heart of active galaxies, see [33]. The jet launching area is most probably the inner part of the accretion disc surrounding the black hole, which is ejected perpendicular to the plane of the accretion disc due to magnetic forces. Until these imaging techniques are feasible - probably in the next few years - we have to wait for direct tests of the redshift effect in the the pc-GR theory. Infrared astronomers hope to detect GR effects, e.g.  $\beta^2$  effects on stellar orbits around the Centre of our Galaxy, Lense-Thirring precession of the orbiting stars as well as flares from the last stable orbit, with the powerful GRAVITY instrument mounted at ESO's Very Large Telescope (VLT) in Chile. The VLT is the world's most advanced optical instrument, consisting of four Unit Telescopes with main mirrors of 8.2m diameter and four movable 1.8m diameter Auxiliary Telescopes. Astronomers can test the redshift effect also if the spa-

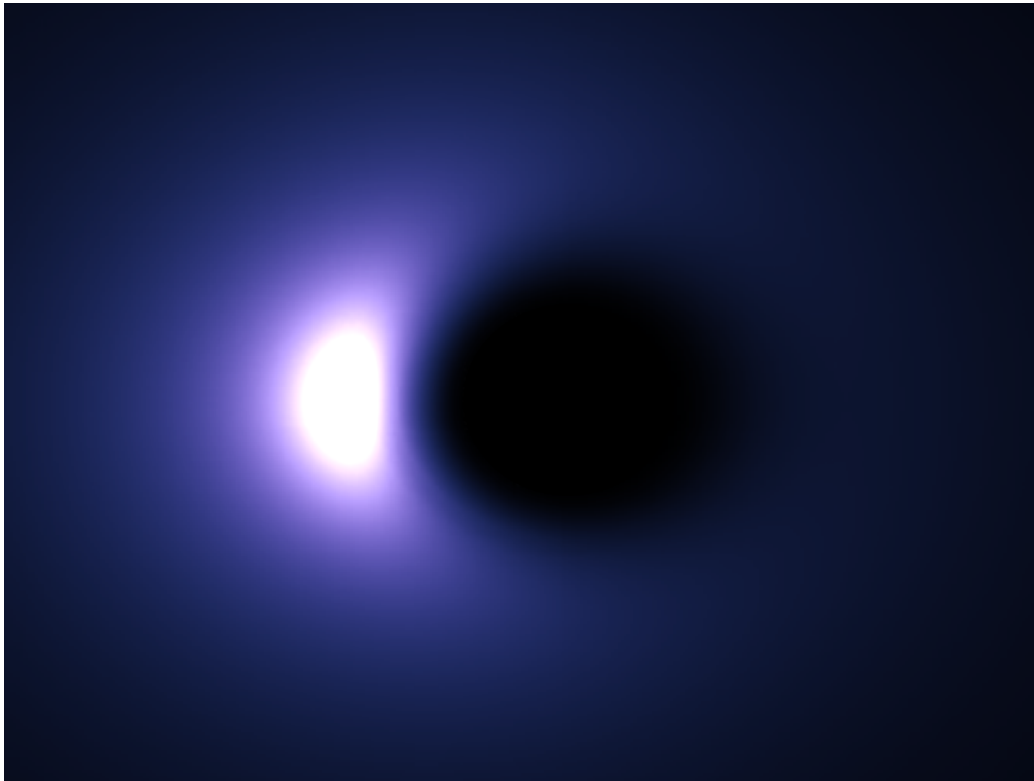


Figure 7: Luminous counter-clockwisely rotating accretion disk around an extremal Kerr black hole (standard GR), see [32]. The inclination angle is 40 degrees. The intensity is color-coded and grows from black (zero emission) over blue to white (maximum emission). On the left-hand side, the bright beaming feature due to Doppler blueshift is clearly visible. The black hole's horizon is seen in the middle of the image.

tial resolution is not high enough. They do this using spectral methods. The spectral techniques are based on the canonical ‘lamppost’ model, see [34]. A hot corona surrounds the central black hole and emits a power law spectrum. The X-rays from the hot corona will also be reflected off the accretion disc resulting in the emission of fluorescent lines. As shown by [27] the shape of the emitted lines gives information about the distance of the line to the black hole, the amount of gravitational redshift and the inclination of the accretion disc. In the rest frame the line is usually well approximated by a Gaussian profile. However, in the observer’s frame various effects influence the line profile, namely the relativistic Doppler effect and the gravitational redshift effect (see e.g. [35]). Hence, the evidence for gravitational redshift can be extracted from the red wing of the line. Typically, the closer the line emitting region extends towards the black hole, the greater the reduction in line emission at the red wing and the greater the reduction in the line flux. This idea was exploited to measure black hole spin because the last stable orbit of a standard Kerr black hole is significantly smaller than for a Schwarzschild black hole, see [36]. The fluorescent lines in the X-ray range are well suited for determining basic parameters of the X-ray emitting regions very close to the central black hole. The most prominent fluorescent line is the strong iron  $K\alpha$  line, visible at 6.4 keV rest frame energy. In a similar energy range there is also a weaker iron L line. These lines are not visible in all black hole candidates, but can be seen for those cases where a cold geometrically thin and optically thick accretion disk is irradiated by hard X-ray radiation from a hot nearby source.

A full solution would require putting the metrics of a pc-Schwarzschild and a pc-Kerr gray star into a ray tracing code which solves the geodesic equation for a number of light rays (i.e. the null geodesic equation). However, this complex task lies beyond the scope of this paper.

Figure 9 shows that a pc-GR Schwarzschild object could mimic a standard Kerr black hole because the last stable orbit is closer to the event horizon in the pc-GR case. This could be measured using iron K lines because fits deliver constraints on the inner disk edges. However, one now has a new situation with maybe completely different spin parameters. Ideally astronomers combine a variety of spin determination methods to constrain robustly the true spin value.

### 3.3 Effective potentials and circular orbits

In this section we derive the effective potential for the radial motion of a geodesic in the equatorial plane, e.g.  $\vartheta = \pi/2$ . For this case the variation of the Lagrangian (4) leads to the following geodesic equations for  $t$  and  $\varphi$ :

$$\begin{aligned} 0 &= \frac{d}{ds} \frac{\partial L}{\partial \dot{t}} = \frac{d}{ds} (2g_{00}c^2\dot{t} + 2g_{03}c\dot{\varphi}) \\ 0 &= \frac{d}{ds} \frac{\partial L}{\partial \dot{\varphi}} = \frac{d}{ds} (2g_{33}\dot{\varphi} + 2g_{03}c\dot{t}) \quad , \end{aligned} \quad (24)$$

which we write as

$$\begin{aligned} g_{00}c\dot{t} + g_{03}\dot{\varphi} &=: \tilde{E} \\ g_{33}\dot{\varphi} + g_{03}c\dot{t} &=: -\tilde{L} \quad , \end{aligned} \quad (25)$$

where  $\tilde{E}$  and  $\tilde{L}$  can be identified with the energy  $\tilde{E} = E/\mu c^2$  and the angular momentum  $\tilde{L} = L/\mu c$  per mass  $\mu$  of a test particle, see [9, p. 266ff.]. An elementary rearrangement yields

$$\begin{aligned} Dc\dot{t} &= -g_{03}\tilde{L} - g_{33}\tilde{E} \\ D\dot{\varphi} &= g_{03}\tilde{E} + g_{00}\tilde{L} \quad , \end{aligned} \quad (26)$$

where we again denote  $D = (-g_{00}g_{33} + g_{03}^2)$ . Inserting equation (26) into equation (4) and simplifying yields

$$\dot{r}^2 = \frac{1}{g_{11}D} \left( \tilde{E}^2 g_{33} + 2g_{03}\tilde{L}\tilde{E} + g_{00}\tilde{L}^2 + D \right) \quad . \quad (27)$$

This can be rewritten as

$$\frac{1}{2}\tilde{E}^2 = \frac{1}{2}\dot{r}^2 + V(r, \tilde{E}, \tilde{L}) \quad (28)$$

with

$$V(r, \tilde{E}, \tilde{L}) = -\frac{1}{2g_{11}D} \left( \tilde{E}^2(g_{33} - Dg_{11}) + 2\tilde{L}\tilde{E}g_{03} + \tilde{L}^2g_{00} + D \right) \quad (29)$$

$$= \frac{\tilde{L}^2}{2r^2} - \left( \frac{m}{r} - \frac{B}{4r^3} \right) \left( 1 + \frac{(\tilde{L} + a\tilde{E})^2}{r^2} \right) + \frac{(1 - \tilde{E}^2)a^2}{2r^2} + \frac{1}{2} \quad (30)$$



Accordingly the radial motion of a geodesic in the equatorial plane is equivalent to the classical motion of a body with unit mass and energy  $\tilde{E}^2/2$  in a complicated effective potential  $V(r, \tilde{E}, \tilde{L})$ . This concept becomes particularly instructive for the Schwarzschild solution. In this case it holds  $a = 0$ , and the effective potential does not depend on  $\tilde{E}$ :

$$V_S(r, \tilde{L}^2) = \frac{1}{2} - \frac{m}{r} + \frac{\tilde{L}^2}{2r^2} - \frac{m\tilde{L}^2}{r^3} + \frac{B}{4} \left( \frac{1}{r^3} + \frac{\tilde{L}^2}{r^5} \right) . \quad (31)$$

The terms  $-m/r$  and  $\tilde{L}^2/r^2$  correspond to the classical gravitational and centrifugal potential, respectively. In GR the negative term proportional to  $1/r^3$  causes the fall of particles into the singularity at  $r = 0$ , which is avoided in pc-GR due to the repulsive potential proportional to  $(1/r^3 + 1/r^5)$ . If we consider a correction of order  $B/r^n$  with  $n > 3$ , in the last term of equation (31) the exponents of  $r$  in the denominator are  $n$  and  $n + 2$ , respectively, and the repelling character of the potential for small  $r$  is even stronger. Also, an increasing  $B$  does not change the qualitative behavior of the potential.

Whilst for the Kerr metric the effective potential is more complicated and depends not only on  $r$  and  $\tilde{L}$ , but also on  $\tilde{E}$ , it can be used to study the motion along geodesics. Of particular importance are circular orbits, which are given by the simultaneous solutions of  $V = \tilde{E}^2/2$  and  $\frac{\partial V}{\partial r} = 0$ . That is, we consider the set of  $r$ -dependent functions  $V(r; \tilde{E}, \tilde{L})$  with parameter values  $\tilde{E}$  and  $\tilde{L}$ . We now vary these parameters until we obtain a curve  $V(r; \tilde{E}(r_c), \tilde{L}(r_c))$  such that this curve takes on a minimum at  $r = r_c$  ( $c$  stands for *circular orbit*) and has the value  $V(r; \tilde{E}(r_c), \tilde{L}(r_c)) = \tilde{E}^2/2$ . The radius  $r_c$  together with the parameters  $\tilde{E}(r_c)$ ,  $\tilde{L}(r_c)$  corresponds to a stable circular orbit. It is convenient to consider the potential  $\hat{V} = V - \tilde{E}^2/2$  rather than  $V$ . The condition for stable circular orbits is then  $\hat{V} = 0$  and  $\frac{\partial \hat{V}}{\partial r} = 0$ , that is the function  $\hat{V}(r; \tilde{E}, \tilde{L})$  has a double root at  $r = r_c$ .

Instead of trying to solve these conditions directly via equation (30) and its derivative, we use  $\omega \dot{t} = \dot{\varphi}$  as introduced in section 3.1 together with equation (26). We get

$$\tilde{E} = -\tilde{L} \frac{cg_{00} + \omega g_{03}}{cg_{03} + \omega g_{33}} . \quad (32)$$

At this point we can use equation (27) for geodesic circular orbits ( $\dot{r} = 0$ )

and insert equation (32):

$$0 = \tilde{L}^2 g_{33} \left( \frac{cg_{00} + \omega g_{03}}{cg_{03} + \omega g_{33}} \right)^2 - \tilde{L}^2 g_{03} \frac{cg_{00} + \omega g_{03}}{cg_{03} + \omega g_{33}} + \tilde{L}^2 g_{00} + D \quad . \quad (33)$$

A rather cumbersome rearrangement of this equation yields (together with equation (32))

$$\begin{aligned} \tilde{L}^2 &= \frac{L^2}{\mu^2 c^2} = \frac{(cg_{03} + \omega g_{33})^2}{g_{33}\omega^2 + 2g_{03}\omega c + g_{00}c^2} \\ \tilde{E}^2 &= \frac{E^2}{\mu^2 c^4} = \frac{(cg_{00} + \omega g_{03})^2}{g_{33}\omega^2 + 2g_{03}\omega c + g_{00}c^2} \quad . \end{aligned} \quad (34)$$

In these equations  $E$  and  $L$  are constants of motion, which correspond to energy and angular momentum of a test particle on a circular geodesic. Both  $E$  and  $L$  have to be real numbers, and accordingly, the right hand side of equation (34) has to be positive. While the numerator is always positive, the denominator corresponds to equation (13) in section 3.1 and thus can be written as

$$g_{33}\omega^2 + 2g_{03}\omega c + g_{00}c^2 = g_{33}(\omega - \bar{\omega}_+)(\omega - \bar{\omega}_-) \quad , \quad (35)$$

where we have used the respective limiting orbital frequencies for general orbits. The factor  $g_{33}$  is always negative, and thus the product  $(\omega - \bar{\omega}_+)(\omega - \bar{\omega}_-)$  has to be negative for  $E^2$  and  $L^2$  to be positive. Recall that in pc-GR  $\bar{\omega}_- > 0$  and  $\bar{\omega}_+ < 0$  (see section 3.1). If  $\omega > 0$ , one has  $(\omega - \bar{\omega}_+) > 0$ , and thus it has to hold  $\omega < \bar{\omega}_-$  for the expression (35) to be positive. For  $\omega < 0$ , the term  $(\omega - \bar{\omega}_-)$  is negative, and the expression (35) is positive for  $\omega > \bar{\omega}_+$ . It follows, that the constraint of positive  $E^2$  and  $L^2$  is equivalent to the constraint, that the orbital frequency  $\omega$  of a stable circular orbit is within the limits given by  $\bar{\omega}_\pm$  derived for general orbits.

We will show now, that for classical GR the conditions  $\hat{V} = 0$  and  $\frac{\partial \hat{V}}{\partial r} = 0$  can only be fulfilled for  $\tilde{E}^2 < 1$ , see [37]. Let us, for the moment, consider the classical GR, from equation (30) with  $B = 0$  and  $\hat{V} = V - \tilde{E}^2/2$  one obtains the expression

$$\begin{aligned} \hat{V}(r, \tilde{E}, \tilde{L}) &= \frac{\tilde{L}^2}{2r^2} - \frac{m}{r} - \frac{m(\tilde{L} + a\tilde{E})^2}{r^3} \\ &\quad + \frac{(1 - \tilde{E}^2)a^2}{2r^2} + \frac{1}{2}(1 - \tilde{E}^2) \quad . \end{aligned} \quad (36)$$

For  $r \rightarrow 0$  it holds  $\hat{V} \rightarrow -\infty$ , which has the consequence that if  $\hat{V}$  has a minimum at  $r_c$  with  $\hat{V}(r_c) = 0$ , there has to be another root in the interval  $(0, r_c)$ .

The roots of  $\hat{V}$  are identical to the roots of the polynomial

$$\begin{aligned} P(r, \tilde{E}, \tilde{L}) &= r^3 \hat{V}(r, \tilde{E}, \tilde{L}) \\ &= \frac{1}{2} (1 - \tilde{E}^2) r^3 - m r^2 \\ &\quad + \frac{1}{2} (\tilde{L}^2 + (1 - \tilde{E}^2) a^2) r - m (\tilde{L} + a\tilde{E})^2 \end{aligned} \quad (37)$$

According to Descartes' rule of signs the number of positive roots is smaller than or equal to the number of variations in the sign in the polynomial, with multiple roots counted separately, see [38]. Given a double root at  $r_c$  and another root in the interval  $(0, r_c)$ , this demands three changes of sign in the polynomial  $P(r, \tilde{E}, \tilde{L})$ . This is only possible if  $\tilde{E}^2 < 1$ . Clearly now, this is a necessary (but not sufficient) condition for the occurrence of a stable circular orbit.

We now turn to the case of pc-GR with  $B \neq 0$ . From equation (30) with  $\hat{V} = V - \tilde{E}^2/2$  we obtain

$$\begin{aligned} \hat{V}(r, \tilde{E}, \tilde{L}) &= \frac{\tilde{L}^2}{2r^2} - \frac{m}{r} - \frac{m (\tilde{L} + a\tilde{E})^2}{r^3} + \frac{(1 - \tilde{E}^2)a^2}{2r^2} \\ &\quad + \frac{1}{2} (1 - \tilde{E}^2) + \frac{B}{4r^3} + \frac{B (\tilde{L} + a\tilde{E})^2}{4r^5} . \end{aligned} \quad (38)$$

For  $r \rightarrow 0$  it holds  $\hat{V} \rightarrow \infty$  (repulsive potential), whereas for  $r \rightarrow \infty$  it approaches  $\frac{1}{2} (1 - \tilde{E}^2)$  from below. It follows that if we have a minimum of  $\hat{V}$  at  $r_c$  with  $\hat{V}(r_c) = 0$ , for  $\tilde{E}^2 \geq 1$  there is another positive root at some value  $r' > r_c$ . In this case and as well for  $\tilde{E}^2 < 1$ , there might be additional roots, but their existence is not a necessary condition for a double root which is a minimum at  $r_c$ .

The roots of  $\hat{V}$  are identical to the roots of the polynomial

$$\begin{aligned}
P(r, \tilde{E}, \tilde{L}) &= r^5 \hat{V}(r, \tilde{E}, \tilde{L}) \\
&= \frac{1}{2} \left(1 - \tilde{E}^2\right) r^5 - m r^4 + \frac{1}{2} \left(\tilde{L}^2 + \left(1 - \tilde{E}^2\right) a^2\right) r^3 \\
&\quad + \left[\frac{B}{4} - m \left(\tilde{L} + a\tilde{E}\right)^2\right] r^2 + B \left(\tilde{L} + a\tilde{E}\right)^2
\end{aligned} \tag{39}$$

For  $\tilde{E}^2 < 1$  there are always two changes of sign in the first three terms. Thus, the necessary condition for the existence of a stable circular orbit is always fulfilled. For  $\tilde{E}^2 > 1$ , the polynomial has to show three changes of sign (recall that the double root at the minimum is counted separately). Therefore, the two conditions

$$\begin{aligned}
\tilde{L}^2 + \left(1 - \tilde{E}^2\right) a^2 &> 0 \\
\frac{B}{4} - m \left(\tilde{L} + a\tilde{E}\right)^2 &< 0 \quad .
\end{aligned} \tag{40}$$

have to hold. It therefore follows, that in pc-GR it is not the general requirement  $\tilde{E}^2 < 1$ , but the weaker restriction (40) for  $\tilde{E}^2 > 1$  that is a necessary condition for the occurrence of stable circular orbits.

There might be various combinations  $r_c, \tilde{E}(r_c), \tilde{L}(r_c)$  corresponding to stable circular orbits. The last stable orbit can be found by setting  $\frac{\partial^2 V}{\partial r^2} \Big|_{r_c} = 0$ . Together with equations (34) and (29) this is equivalent to

$$\begin{aligned}
&g_{33}''(g_{00} + \omega g_{03})^2 + g_{00}''(g_{03} + \omega g_{33})^2 \\
&\quad - 2g_{03}''(g_{00} + \omega g_{03})(g_{03} + \omega g_{33}) \\
&\quad + D''(\omega^2 g_{33} + 2\omega g_{03} + g_{00}) = 0 \quad .
\end{aligned} \tag{41}$$

Unfortunately equation (41) has a quite complicated form when we insert

the pc-Kerr metric [done with [39]]

$$\begin{aligned}
& \frac{1}{r(4r^5 + a^2(3B - 4mr^2))^2} \left[ -6a^4(15B^2r - 32Bmr^3 + 16m^2r^5) \right. \\
& \pm 4ar^{5/2}\sqrt{-3B + 4mr^2}(15B^2 + 24mr^4(2m + r) - 10Br^2(4m + 3r)) \\
& + 4r^5(-15B^2 + 8mr^4(-6m + r) + 2Br^2(20m + 3r)) \\
& + a^2(45B^3 - 18B^2r^2(10m + 17r) - 96mr^6(2m^2 + 5mr + r^2) \\
& + 8Br^4(38m^2 + 96mr + 15r^2)) \\
& \left. \pm 8a^3\left(4mr^{9/2}(4m + 3r)\sqrt{-3B + 4mr^2} \right. \right. \\
& \left. \left. - 3Br^{5/2}(8m + 5r)\sqrt{-3B + 4mr^2} + 9B^2\sqrt{-3Br + 4mr^3}\right) \right] = 0 \quad . \quad (42)
\end{aligned}$$

For  $B = 0$  this equation greatly simplifies to [done with [39]]

$$r^2 - 6mr \pm 8a\sqrt{mr} - 3a^2 = 0 \quad , \quad (43)$$

which is the same as in [40]. The upper sign here refers to a co-rotating object. Up to now we have not found analytical solutions for equation (42). Numerical investigations showed, that equation (42) has two solutions for counter-rotating objects (see Fig. 8). However only the outer one of these solutions is physically relevant as one has to consider the constraints given by equation (14). The origin of the complex structure of the last equation is the addition of the  $B/(2r^3)$  term in the metric, resulting in a new rich structure of solutions.

Equation (42) also has two solutions for co-rotating objects but only up to a value of  $a > -0.416m$  (see Fig. 9). For higher absolute values of  $a$ , equation (42) has no positive real roots for co-rotating objects. For this case, the second derivative of the potential is always positive, i.e., *a stable orbit always exists*.

As we encounter a new physical phenomenon, namely the existence of two critical orbits compared to only one in the classical Kerr metric, we will investigate Fig. 9 a little bit further.

To do so we divide the illustrated parameter space into four different regions:

- I This region is bounded by the solid line which represents the last stable orbit in GR. For all combinations of  $a$  and  $r$  above this line  $\frac{\partial^2 V}{\partial r^2}$  is positive for both GR and pc-GR. Thus, in this region there exist stable circular orbits in both theories.

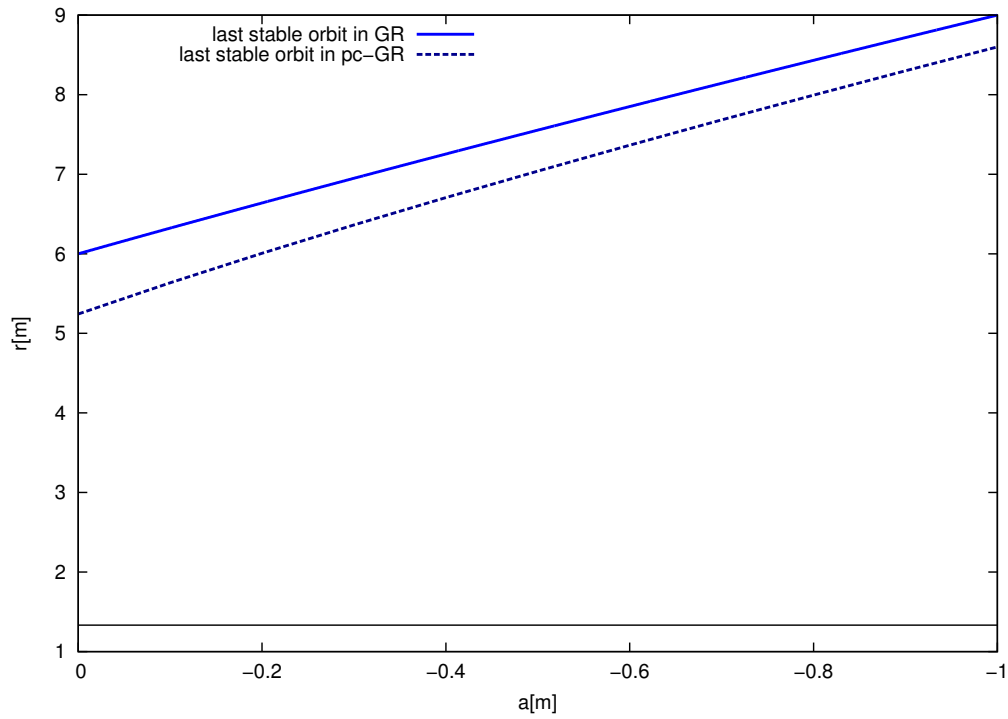


Figure 8: Critical stable orbits for retrograde test masses - the parameter  $B$  is set to  $B = \frac{64}{27}m^3$ .

- II In this area  $\frac{\partial^2 V}{\partial r^2}$  is positive for pc-GR, in contrast to standard GR where  $\frac{\partial^2 V}{\partial r^2}$  is negative. This means that for all combinations of  $r$  and  $a$  in this dark shaded area there are stable circular orbits in pc-GR but not in GR.
- III Here, between the dashed and dash-dotted curves,  $\frac{\partial^2 V}{\partial r^2}$  is negative for all values of  $r$  and  $a$  even for pc-GR. So there are no stable geodesic circular orbits in this light shaded area regardless of the theory concerned.
- IV In principle, orbits would be stable here for pc-GR,  $\frac{\partial^2 V}{\partial r^2}$  is positive in this region, but the constraint (14) excludes this area for general orbits (i.e.  $ds^2$  is negative in this area).

The most interesting area now is II as we do have a different behavior for pc-GR compared to GR. In this region there exist stable orbits in pc-GR but not in GR. Especially for values of  $a < -0.416m$  we have  $\frac{\partial^2 V}{\partial r^2} > 0$  for all values of  $r$  which means that here no last stable orbit occurs but rather all orbits are stable in pc-GR. Going to values of  $a > -0.416$  we also see a new phenomenon. In contrast to GR there now exists an area of unstable orbits which has an upper (dashed curve - corresponds to the solid curve in GR) and lower (dash-dotted curve - not existent in GR) bound. Thus, in pc-GR there is a ring-shaped area of unstable orbits with a stable zone in the middle around the central mass while in GR this area is a disc extending to the surface of the black hole with no stable zone below the last stable orbit.

For radii smaller than  $\frac{4}{3}m$  the solutions of equation (8) become imaginary. However,  $r = \frac{4}{3}m$  is the position of the global minimum of  $g_{00}$  (and therefore the effective potential), describing the final radius of a large mass. For a description at smaller radial distances, the distribution of the object's mass has to be included.

In summary, the physical behavior in pc-GR for counter-rotating orbits is not very different to the standard GR except that the last stable orbit is a little closer to the central mass. For co-rotating orbits however we get a new physical behavior.

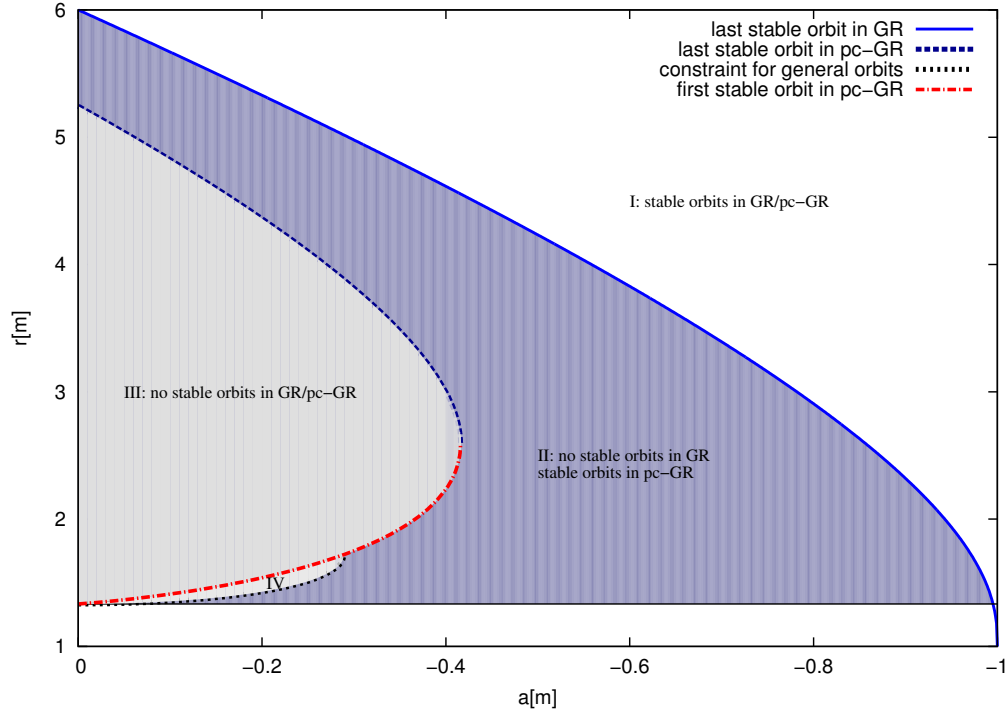


Figure 9: Critical stable orbits for prograde test masses (The curves describe from top to bottom: 1. The last stable orbit in standard GR (thick solid), 2. the ‘last’ stable orbit in pc-GR (dashed), 3. the ‘first’ stable orbit in pc-GR (dash-dotted), 4. the limit to general orbits given by equation (14) (dotted) and 5. the point where the pc-equations become imaginary ( $r = \frac{4}{3}$ , thin solid)). We now have to distinguish between four different areas. In the unshaded area (I) orbits are stable both in GR and pc-GR, whereas in the dark shaded area (II) orbits are only stable in pc-GR. Both lighter shaded areas (III and IV) do not contain stable orbits at all. The plot is done for a value of  $B = \frac{64}{27}m^3$ .



## 4 Conclusions and outlook

We have identified several observables and proposed associated possibilities for astronomical measurements, which may distinguish between different predictions of pseudo-complex General Relativity and standard GR. For distances comparable to the Schwarzschild radius we showed that the angular frequencies and allowed orbits of particles orbiting around a dense central object ('gray star' in pc-GR or black hole in GR) and the gravitational redshift differ significantly between GR and pc-GR. We have illustrated that the observables related to the orbital frequency may be accessible by measuring plasma clouds or flares from the vicinity of a gray star/black hole. We also showed how techniques to determine the gravitational redshift close to the central object could be applied.

These are our new findings: For particles moving in the equatorial plane the angular frequencies for pro- and retrograde geodesic orbits in pc-GR metrics are smaller than those for particles moving according to GR. We found that the limits of the angular frequency for general circular motions in the equatorial plane to have a wider range in pc-GR than in GR leading to a weaker frame dragging effect. Therefore, we propose to measure plasma clouds or flares close to the Galactic center or M87. We elaborated the differences between pc-GR and GR considering the redshift of an emitting particle at rest. We found that the redshift in pc-GR is smaller than in GR for central objects with the same mass and density. Especially the poles of rotating dense objects are much brighter, so that the inclination has a pronounced effect on the blackness of the central star. To observe this, we proposed to directly investigate the optical appearance of the dense object preferably by radio astronomy or by using spectral methods e.g. tracing of X-ray iron lines. Finally, we considered the effective potentials of the GR and pc-GR geometries and their impact on the allowed circular orbits. By deriving the effective potentials and introducing the requirements for stability of circular orbits, we discussed the restraints of the angular momentum and the energy, so that we could identify the stable orbits in pc-GR and GR. We showed, that in pc-GR the concept of one last stable orbit is changed. Depending on the momentum of the central mass there is a last stable orbit ( $a = 0$ ) and it exists a forbidden zone between a 'last' and a 'first' stable orbit (at a certain point below the 'last' stable orbit orbits get stable again;  $0 > a > -0.416m$ ) or for all radii a stable orbit can be found ( $a < -0.416m$ )!

Here, we have shown how the pseudo-complex General Relativity changes the standard picture. We presented various predictions of pc-GR in the vicinity of black-hole candidates which are testable with astronomical methods. The field of pc-GR is rather new, hence there are still many open questions. Among them are other aspects yet to be investigated like the significance of pc-GR at a cosmological length scale as well as its implications at a microscopic scale.

## Acknowledgments

The authors express sincere gratitude for the possibility to work at the *Frankfurt Institute of Advanced Studies* and at the *GSI* with their excellent working atmosphere. Peter Otto Hess also acknowledges financial support from FIAS, DGAPA-PAPIIT (IN103212), DGAPA and CONACyT. Gunther Caspar acknowledges financial support from *Frankfurt Institute for Advanced Studies*. Thomas Schöenbach acknowledges support from *Stiftung Polytechnische Gesellschaft Frankfurt am Main*. Andreas Müller acknowledges support by the DFG cluster of excellence 'Origin and Structure of the Universe'. Thomas Boller is grateful to Stefan Gillessen for intensive discussion on the Galactic Center research lead by the infrared group of the Max-Planck-Institute for extraterrestrial physics. The authors thank Tom Dwelly for critical reading of the paper.

## References

- [1] Hess P. O., Greiner W., 2009, Int. J. Mod. Phys. E 18, 51
- [2] Caspar G. et al., 2012, Int. J. Mod. Phys. E Vol. 21, No. 2
- [3] Kelly P. F., Mann R. B., 1986, Class. and Quant. Grav, 3, 705
- [4] Hess P. O., Maghlaoui L., Greiner W., 2010, Int. J. Mod. Phys. E 19, 1315
- [5] Genzel R. et al., 2003, Nature, Volume 425, Issue 6961, 934
- [6] Aschenbach B. et al., 2004, A&A 417, 71
- [7] Iwasawa K., Miniutti G., Fabian A.C., 2004, MNRAS, 355, 1073

- [8] Gillessen S. et al., 2012, *Nature*, Volume 481, 51
- [9] Adler R., Bazin M., Schiffer M., 1975, *Introduction to General Relativity*, McGraw Hill, New York
- [10] Antonuccio F., 1994, preprint (gr-qc/9311032)
- [11] Kantor I. L., Solodovnikov A. S., 1989, *Hypercomplex Numbers. An Elementary Introduction to Algebra*, Springer, Heidelberg
- [12] Misner C. W., Thorne K. S., Wheeler J. A., 1973, *Gravitation*, W. H. Freeman Company, San Francisco
- [13] Schuller F. P., 2003, PhD thesis, Cambridge
- [14] Schuller F. P., Wohlfarth M. N. R., Grimm T. W., 2003, *Class. Quantum Grav.* 20, 1
- [15] Visser M., 1996a, *Phys. Rev. D* 54, 5103
- [16] Visser M., 1996b, *Phys. Rev. D* 54, 5116
- [17] Visser M., 1997, *Phys. Rev. D* 57, 936
- [18] Will C. M., 2006, *Living Rev. Relativity* 9, 3 [Online Article]: <http://www.livingreviews.org/lrr-2006-3>.
- [19] Mazur P. O., Mottola E., 2004, *PNAS*, vol. 101, Issue 26, p.9545-9550
- [20] Müller A., Camenzind M., 2004, *A&A*, Volume 413, Number 3, 861-878.
- [21] Lense J., Thirring H., 1918, *Phys. Z.* 19, 156.
- [22] Ciufolini I., Pavlis E. C., 2004, *Nature*, Volume 431, 958.
- [23] Everitt C. W. F. et al., 2011, *Phys. Rev. Lett.* Volume 106, Issue 22
- [24] Gezari S. et al., 2006, *Astrophys. J.* 653, L25
- [25] Komossa S. et al., 2004, *Astrophys. J.* 603, L17
- [26] Rees M., 1988, *Nature* 333, 523
- [27] Müller A., Wold M., 2006, *A&A* 457, 485

- [28] Gillessen S. et al., 2009, ApJ 707, 114
- [29] Eisenhauer F. et al., 2011, The Messenger, vol. 143, p. 16-24
- [30] Nandra K., 2011, in The X-ray Universe 2011, Presentations of the Conference held in Berlin, Germany, ATHENA: The Advanced Telescope for High Energy Astrophysics
- [31] Boller Th., Müller A., 2012, in Symposium on Exciting Physics: quarks and gluons /atomic nuclei / biological systems /networks, Makutsi Safari Farm, South Africa, submitted
- [32] Müller A., 2007, in School on Particle Physics, Gravity and Cosmology, 21.08.-02.09.06 in Dubrovnik, published in: Proceedings of Science (P2GC) 017; Editors: Bonora L., Fajfer S., Iengo R., Klabucar D., Palua S., Picek I.
- [33] Krichbaum T. P., Zensus J. A., Witzel A., 2005, Astron. Nachr. 326, 548
- [34] George I.M., Fabian A.C., 1991, MNRAS 249, 352
- [35] Müller A., Camenzind M., 2004, A&A 413, 861
- [36] Tanaka Y. et al., 1995, Nature 375, 659-661
- [37] Wilkins D. C., 1972, Phys. Rev. D 5, 814
- [38] Anderson B., Jackson J., Sitharam M., 1998, Amer. Math. Monthly 105, 447
- [39] Wolfram Research Inc., 2011, Mathematica, Version 8.0.1.0, Champaign, IL
- [40] Bardeen J. M., Press W. H., Teukolsky S. A., 1972, Astrophysical J., Vol. 178, pp. 347-370